ADVANCED FUNCTIONAL MATERIALS
www.afm-journal.de

Wafer Scale Synthesis and High Resolution Structural Characterization of Atomically Thin MoS_2 Layers

*Aaron S. George, Zafer Mutlu, Robert Ionescu, Ryan J. Wu, Jong S. Jeong, Hamed H. Bay, Yu Chai, K. Andre Mkhoyan, Mihrimah Ozkan, and Cengiz S. Ozkan**

Synthesis of atomically thin MoS_2 layers and its derivatives with large-area uniformity is an essential step to exploit the advanced properties of MoS_2 for their possible applications in electronic and optoelectronic devices. In this work, a facile method is reported for the continuous synthesis of atomically thin MoS_2 layers at wafer scale through thermolysis of a spin coated-ammonium tetrathiomolybdate film. The thickness and surface morphology of the sheets are characterized by atomic force microscopy. The optical properties are studied by UV–Visible absorption, Raman and photoluminescence spectroscopies. The compositional analysis of the layers is done by X-ray photoemission spectroscopy. The atomic structure and morphology of the grains in the polycrystalline MoS_2 atomic layers are examined by high-angle annular dark-field scanning transmission electron microscopy. The electron mobilities of the sheets are evaluated using back-gate field-effect transistor configuration. The results indicate that this facile method is a promising approach to synthesize MoS_2 thin films at the wafer scale and can also be applied to synthesis of WS_2 and hybrid MoS_2-WS_2 thin layers.

1. Introduction

Atomically thin two-dimensional (2D) transition-metal dichalcogenide (TMD) materials (MoS_2, WS_2, $MoSe_2$, WSe_2, NbS_2, $NbSe_2$, etc.) hold promise for next-generation electronics due to enticing optical and electronic properties.[1] TMD materials exhibit a large variety of electronic behaviors such as metallic, semiconductivity and superconductivity.[2–4] MoS_2, a semiconducting TMD material, possesses an indirect band gap of ≈1.3 eV in its bulk form and a direct band gap of ≈1.8 eV as a monolayer, allowing its realization in advanced optoelectronic devices.[5,6] Moreover, large on/off current ratio (10^8) and abrupt switching (sub-threshold swing ≈70 mV/decade) have been recently reported for monolayer MoS_2 transistors, suggesting promise in future electronic devices such as low power applications.[7–9] In this regard, synthesis of large uniform area atomically thin MoS_2 films by a facile and reliable method is an essential requirement for applying these novel electronic and optical properties into future electronic and optoelectronic devices.

Recent top-down approaches such as micromechanical exfoliation, liquid exfoliation and intercalation assisted exfoliation to obtain large-area MoS_2 thin films have received considerable attention.[10–12] However, lateral dimensions of films from these methods have been reported to be tens of micrometers, which limits their applications for large-area electronics.

Using elemental S and MoO_3, Najmaei et al.[13] and Zande et al.[14] have recently demonstrated the bottom-up growth of centimeter scale highly crystalline MoS_2 films via chemical vapor deposition (CVD). Although this approach is promising for future production of MoS_2, current production of MoS_2 at wafer scale is still in a nascent stage.

Other techniques for synthesis of MoS_2 reported in the literature include thermolysis of single precursor containing M and S and sulfurization of MoO_3 films.[15–19] Synthesis of MoS_2 films was reported by thermolysis of the spin casted-$(NH_4)_2MoS_4$ or alkyldiammonium thiomolybdate a decade ago, but with several nanometers in thickness and undesirable carbon residues.[15] More recently, MoS_2 films have been synthesized by thermolysis of dip-coated $(NH_4)_2MoS_4$ films on sapphire under sulfur pressure and transferred to SiO_2.[17]

In this report, we have demonstrated direct synthesis of atomically thin MoS_2 sheets on SiO_2/Si at wafer scale by thermolysis of spin coated-$(NH_4)_2MoS_4$ films. Spin coating of the films offers excellent control of the film thickness by varying the concentration of solution and spin coating speed.

A. S. George, Z. Mutlu, Y. Chai
Materials Science and Engineering Program
University of California
Riverside, CA 92521, USA
R. Ionescu
Department of Chemistry
University of California
Riverside, CA 92521, USA
R. J. Wu, J. S. Jeong, Prof. K. A. Mkhoyan
Department of Chemical Engineering & Materials Science
University of Minnesota
Minneapolis, MN 55455, USA
Prof. M. Ozkan
Department of Electrical Engineering
University of California
Riverside, CA 92521, USA
H. H. Bay, Prof. C. S. Ozkan
Department of Mechanical Engineering
University of California
Riverside, CA 92521, USA
E-mail: cozkan@engr.ucr.edu

DOI: 10.1002/adfm.201402519

© 2014 WILEY-VCH Verlag GmbH & Co. KGaA, Weinheim

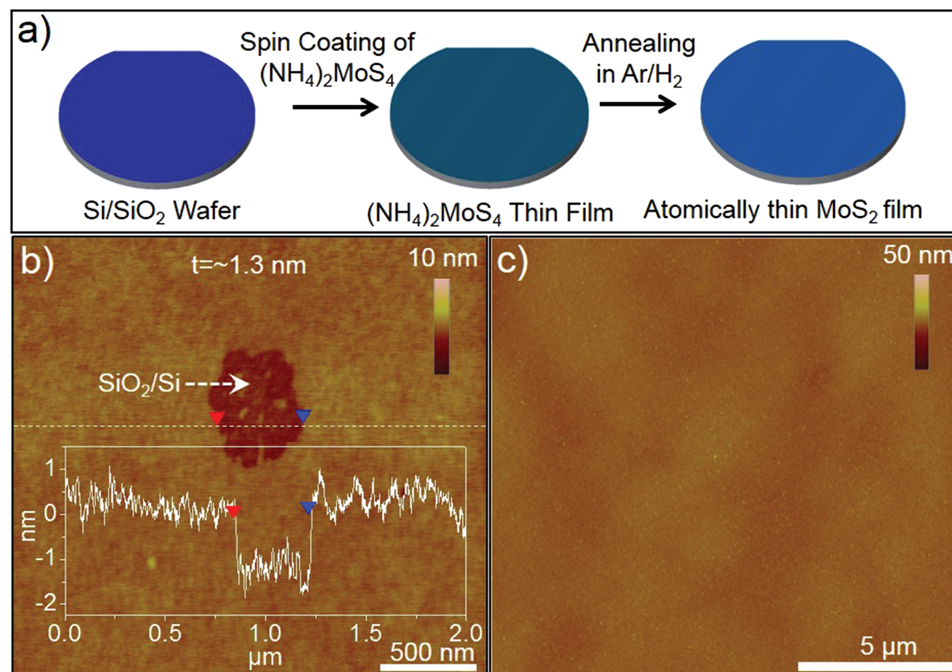

Figure 1. a) Schematic representation of the preparation procedure of atomically thin MoS_2 films at wafer scale. AFM images and height profiles of the MoS_2 film in b) a dewetted region and c) a continuous region.

Additionally, thermolysis of the spin coated thin films offers a method to synthesize MoS_2 sheets without the use of sulfur and high temperatures.

2. Results and Discussion

2.1. Thickness and Surface Morphology

Figure 1a schematically illustrates the preparation procedure of atomically thin MoS_2 films. Our approach is based on the thermolysis of spin coated-$(NH_4)_2MoS_4$ films to grow MoS_2 thin layers on SiO_2/Si at wafer scale. Atomic force microscopy (AFM) was used to characterize the surface morphology and thickness of MoS_2 thin layers. Figure 1b shows the AFM image and height profile of the MoS_2 film with a dewetted region, which is occasionally observed on the film. The thickness of the film is measured from the edges of the dewetted region. The inset shows that the thickness of the film is ≈1.3 nm, a value consistent with the expected thickness from a bilayer MoS_2.[20] The surface roughness value, Ra, is determined to be 0.25 nm from the height profile in Figure 1c.

2.2. Atomic Structure Characterization

High-angle annular dark-field scanning TEM (HAADF-STEM) images of the MoS_2 film at different magnifications are shown in **Figure 2**. Regions of monolayers as well as double and triple layers can be identified here consistent with AFM and Raman analysis.[21] Thicker regions, containing two or three layers, appear more intense in these images because the higher number of atoms in each atomic column leads to higher scattering of the incident electron beam into ADF detector. Figure 2c shows the characteristic hexagonal structure of MoS_2.

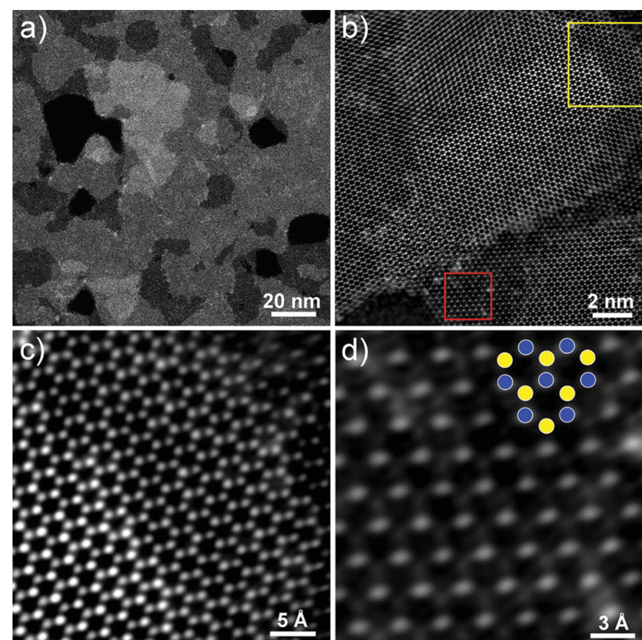

Figure 2. HAADF-STEM images of MoS_2 film: a) low magnification; b) intermediate magnification; c) yellow box section of panel b showing thickness steps resulting in tri-, bi- and monolayer (left to right); d) red box section of panel b showing monolayer MoS_2 with slight carbon residue (cloudy spots) with overlaid model: Mo-blue and S-yellow. All images have been filtered using 0.25 $Å^{-1}$ low-pass filter keeping Fourier peaks up to 0.9 $Å^{-1}$.

© 2014 WILEY-VCH Verlag GmbH & Co. KGaA, Weinheim

Two atomic sites with distinguishable intensities can be identified at each thickness step as a result of the AB stacking of the MoS_2 structure, proving that the material is indeed semiconducting 2H polymorph and not metallic 1T.[21] For the monolayer 2H MoS_2 (Figure 2d), the higher intensity atoms are Mo, while lower intensity atoms are S as expected for HAADF-STEM imaging. We also did a detail analysis of the grain/domain sizes of the $MoSe_2$ sheets, as shown in Figure S1 (Supporting Information). Basically, the average grain/domain size in these MoS_2 sheets is 25.9 ± 14.7 nm.

2.3. Spectroscopic and Optical Properties

X-ray photoemission spectroscopy (XPS) was used to determine the chemical compositions and chemical states of the precursor and obtained films. **Figure 3**a,b display XPS data for Mo and S binding energies, respectively, from MoS_2 and $(NH_4)_2MoS_4$ films. The $(NH_4)_2MoS_4$ film exhibits two Mo 3d peaks at 232.2 and 235.5 eV, corresponding to the $3d_{3/2}$ and $3d_{5/2}$ binding energies, respectively, characteristic for the Mo^{6+} state.[18] The MoS_2 layer also exhibits two characteristic Mo 3d peaks at 229.3 and 232.5 eV, corresponding to the $3d_{3/2}$ and $3d_{5/2}$ binding energies for the Mo^{4+}, respectively.[22,23] Moreover, a shift in the binding energies of sulfur is also observed. The sulfur peak for the 2s orbital is shifted from 229.2 to 226.6 eV, while $2p_{3/2}$ and $2p_{5/2}$ peaks are shifted from 235.6 to 232.5 eV, and 232.5 to 229.3 eV, respectively, as shown in Figure 3a,b. Decreases in the binding energy of sulfur can be explained by the change of oxidation state of Mo from Mo^{6+} to Mo^{4+}, which causes a decrease in the bond strength between molybdenum and sulfur. The results confirm the change of oxidation state of Mo from Mo^{6+} to Mo^{4+} and the complete transition from $(NH_4)_2MoS_4$ to MoS_2.

Raman spectroscopy is a powerful nondestructive characterization tool to reveal the crystallinity and thickness of 2D atomically thin materials such as TMDs and graphene.[24,25] Figure 3c shows the Raman spectra taken from the regions with various thickness on the MoS_2 film at room temperature. The spectrum reveals two characteristic Raman modes of MoS_2, E_{2g} and A_{1g}. The frequency difference between E_{2g} and A_{1g} phonons has been shown as an indicator of the number of layers in MoS_2.[26,27] We observe the frequency difference of the E_{2g} and A_{1g} peaks to be 19.3 cm^{-1}, corresponding to monolayer MoS_2.[3,6] Other areas of the MoS_2 film show a red shift of E_{2g} peak and blue shift of A_{1g} peak, causing increasing peak spacing between E_{2g} and A_{1g} modes as the number of layers in the MoS_2 thin film increases, indicating the presence of other few-layer regions. The Raman spectra results indicate that 1, 2 and 3 layers can be dominant in different regions of the synthesized film.

To further investigate the quality of MoS_2 films, photoluminescence (PL) and absorption spectroscopy measurements were performed at room temperature. The PL spectrum in Figure 3d reveals an intense peak at 1.84 eV, confirming the

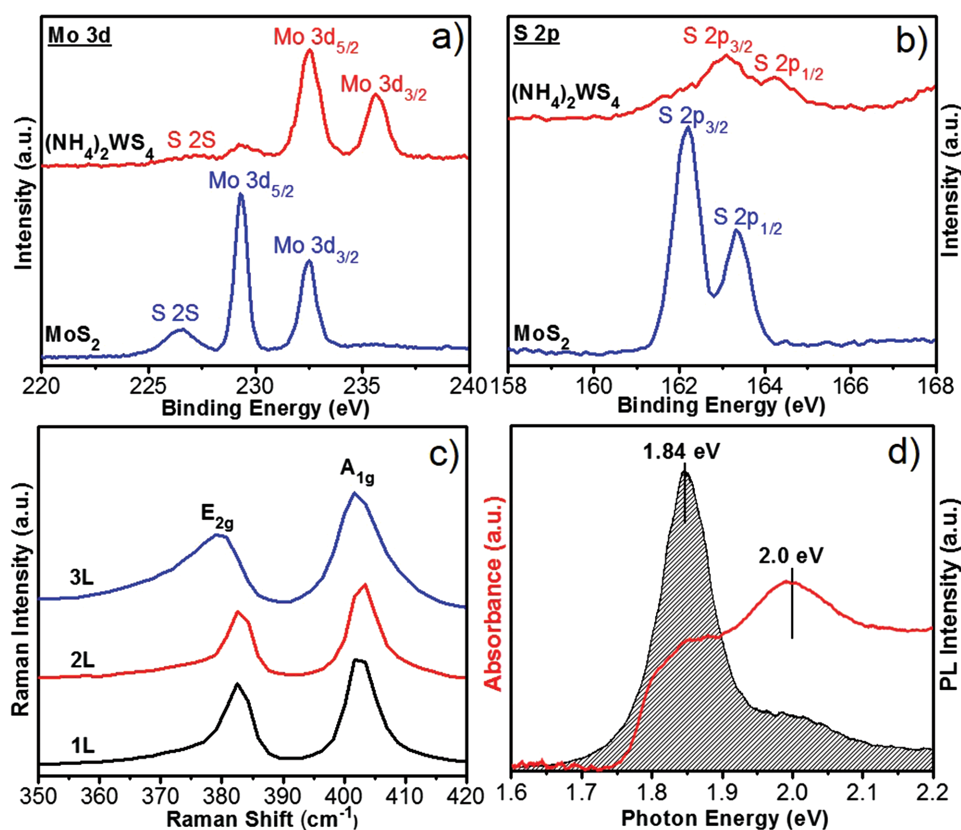

Figure 3. XPS data of a) Mo and b) S binding energies from the MoS_2 and $(NH_4)_2MoS_4$ films. c) Raman spectra from 1, 2 and 3 MoS_2 layers on the film. d) PL and absorption spectra from the film.

© 2014 WILEY-VCH Verlag GmbH & Co. KGaA, Weinheim

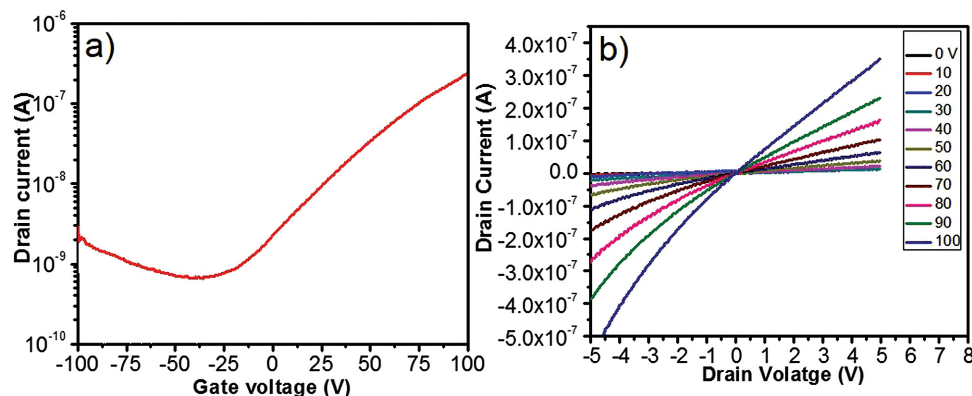

Figure 4. a) Plot of drain current vs gate voltage shows electron transport using Ti/Au contacts, where V_{DS} = 2 V. The on/off ratio for this device is ≈3 × 10^2. b) Drain current vs drain-source voltage characteristics.

presence of the direct band gap in atomically thin MoS_2.[28,29] Figure 3d also shows the absorption spectra of the MoS_2 film. The spectra reveals two absorption peaks at 1.84 eV and 2.0 eV, corresponding to the A1 and B1 direct excitonic transitions at the Brillouin zone K point.[30,31]

2.4. Electrical Properties

To evaluate the electrical transport properties of the films, the few-layer MoS_2 (~1.3 nm) field-effect transistors (FETs) were fabricated on Si/SiO_2 substrates with Ti/Au (10/80 nm) contacts. The corresponding transfer and output plots are shown in **Figure 4**. The field-effect mobility was extracted using the equation $\mu = (dI_d/dV_g)/(\varepsilon V_d W/L_{ox}L)$ (where L_{ox} is the gate dielectric thickness (300 nm), W and L represent channel width and channel length, respectively, ε is the dielectric constant of gate dielectrics (thermal oxide = 3.9) and dI_d/dV_g is the slope calculated from Figure 4a.[3] We found the mobility of MoS_2 from this growth method to be ≈0.1 cm^2 V^{-1} s^{-1}, which is in agreement of earlier reports on the characterization of MoS_2 layers synthesized by the CVD method.[3,6,32] The on/off current ratio is ≈108, which may be increased for $V_g > 100$ V. The transfer plot shows n-type switching behavior of the synthesized MoS_2 thin sheets. The threshold voltage (V_{th}) obtained by linear extrapolation method is ≈70 V. By using the equation $n_{2D} = C_{ox}(V_g - V_{th})/q$ (where C_{ox} is the oxide capacitance), the estimated electron concentration is 7.19 × 10^{11} cm^{-2} at V_g = 80 V and 2.16 × 10^{12} cm^{-2} at V_g = 100 V.

2.5. Growth of WS_2 and Hybrid MoS_2-WS_2 Thin Layers

To demonstrate the versatility of the method described above, we have performed the synthesis of WS_2 from ammonium tetrathiotungstate, $(NH_4)_2WS_4$, in a similar manner to that of MoS_2. The Raman spectra reveals two main characteristics peaks, E_{2g} and A_{1g}, of WS_2, shown by **Figure 5**a.[33] PL spectrum shows an excitation centered at 2.0 eV (Figure 5b).[5,34] Both Raman and PL spectroscopy results confirm the atomically thin film nature of the grown films by this technique.[34–36] Hybrid MoS_2-WS_2 materials can be also synthesized with this approach by simply combining precursors $(NH_4)_2MoS_4$ and $(NH_4)_2WS_4$ in solution prior to spin coating, as confirmed by the Raman spectra in Figure 5c.[37–39] After thermolysis of the two precursor film, an alloy in the form of $Mo_xW_{2-x}S_2$ can be achieved, where x denotes the proportion of Mo and W in the resulting film. PL of the hybrid MoS_2-WS_2 film produced by equal amounts of $(NH_4)_2MoS_4$ and $(NH_4)_2WS_4$ shows an excitation at 1.85 eV, consistent with previous reports of $Mo_xW_{2-x}S_2$ films.[40] It is straightforward to envision how this process can be utilized to achieve homogenous alloys and doping of TMDs.[41]

3. Conclusion

In summary, we have demonstrated the synthesis of MoS_2 layers by the thermolysis of spin coated thin films on the wafer scale. Furthermore, we have shown that samples may be prepared down to monolayer thickness, as revealed by TEM analysis. Back-gate FET devices are fabricated directly on the Si/SiO_2 substrate used for growth and show mobilities of 0.1 cm^2 V^{-1} s^{-1}. This approach may be applied to numerous substrates and suggests a promising route towards the production of other TMD materials, alloyed or electronically doped TMD materials. Thin WS_2 and hybrid MoS_2-WS_2 films have been produced successfully with this method, as confirmed by Raman spectroscopy, offering synthesis of TMD materials with tunable bandgap for future electronics applications. This process provides smooth and relatively uniform synthesis by a facile method, which can exclude the use of elemental sulfur, showing promise in atomically thin TMD synthesis for future electronics applications.

4. Experimental Details

Materials Processing: Herein, atomically thin MoS_2 films were synthesized onto 2 inch SiO_2/Si wafers by thermolysis of spin coated films (see Figure 1a). Precursor solutions were prepared by dissolution of $(NH_4)_2MoS_4$ in n-methylpyrollidone (NMP). Prior to spin coating, wafers were cleaned by sonication in toluene, acetone and isopropanol, sequentially for 45 min each. Next, the substrates were submersed in RCA clean SC-1 (5 parts DI water, 1 part NH_4OH, 1 part H_2O_2) for 15 min. Each step is followed by a DI water rinse.

© 2014 WILEY-VCH Verlag GmbH & Co. KGaA, Weinheim

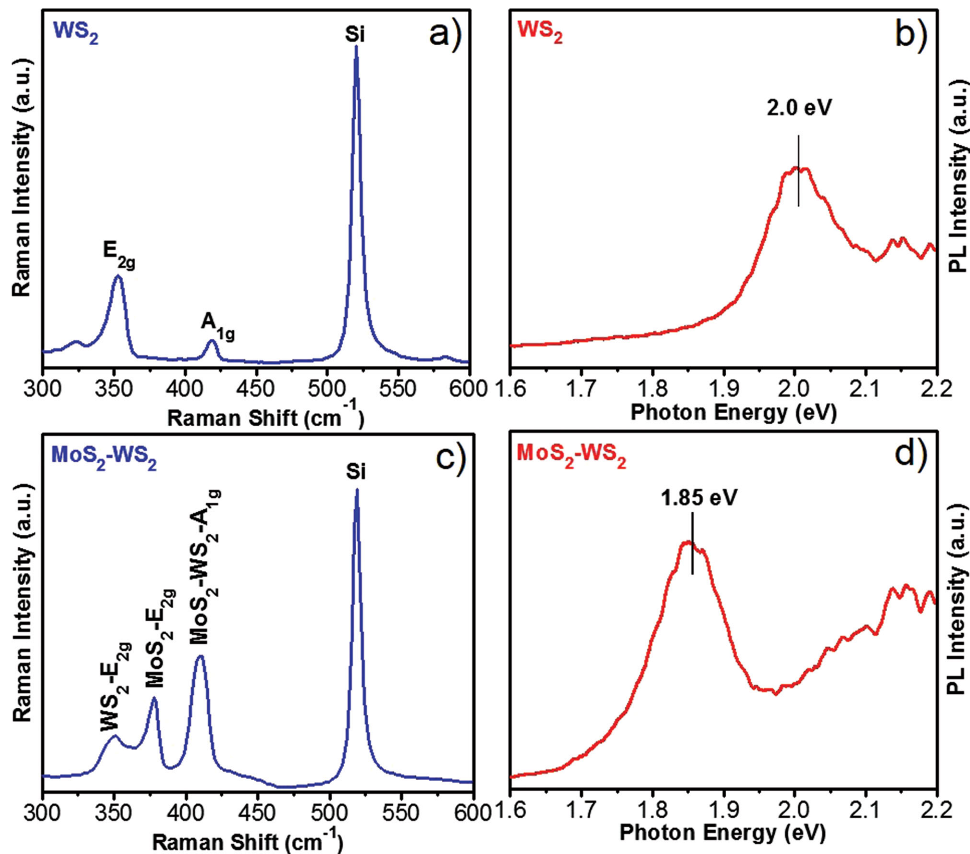

Figure 5. a,c) Raman and b,d) PL spectra of WS_2 and $Mo_xW_{2-x}S_2$ film, respectively.

Immediately, following the cleaning procedure, the precursor films were deposited by spin coating under ambient conditions at 3000 rpm for 1 min. After spin coating deposition, the samples were moved immediately into a CVD furnace and heated to 100 °C under vacuum to remove residual NMP. To complete the thermolysis, samples were annealed under Ar/H_2 gas flow (200/400 sccm) at 480 °C for 1 h. Subsequently, samples were annealed at 1000 °C in Ar gas flow to improve crystallinity.

Materials Characterization: AFM imaging and thickness measurements were performed in tapping mode using a commercial system (Multimode, Veeco). Chemical compositions of the films were determined using a XPS system (Kratos Axis Ultradld) equipped with an Al Kα monochromated X-ray source and a 165-mm electron energy hemispherical analyzer. The vacuum pressure was kept below 3 × 10^{-9} Torr, and a neutralizer was applied during the data acquisition. Raman and PL spectra of the MoS_2 films were collected with a Horiba LabRAM HR spectrometer with excitation wavelength of 532 nm and a laser power of ≈1 mW. The measurements were performed in a confocal micro configuration using a 100× microscope objective lens. Absorbance measurements were performed using a UV–Vis system (Perkin Elmer, Lambda 35). For transmission electron microscopy (TEM), MoS_2 sheets were coated in a protective PMMA layer by spin coating prior to the etching of SiO_2 in 45% KOH. Following transfer to lacey carbon TEM grids and drying, PMMA was removed by submersion in acetone. HAADF-STEM imaging was performed on a FEI Titan G^2 60–300 aberration-corrected STEM equipped with a CEOS DCOR probe corrector operated at 200 kV. The MoS_2 FETs were fabricated directly on the Si/SiO_2 substrate in a backgate FET configuration with Ti/Au (10/80 nm) contacts by using a conventional photolithographic process. DC *I–V* characteristics were obtained at room temperature using an Agilent 4155C semiconductor parameter analyzer with fabricated probe station.

Supporting Information

Supporting Information is available from the Wiley Online Library or from the author.

Acknowledgements

Financial support for this work was provided by the STARnet center C-SPIN (Center for Spintronic Materials, Interfaces, and Novel Architectures), through the Semiconductor Research Corporation sponsored by MARCO and DARPA. XPS data was acquired with equipment funded by the U.S. National Science Foundation under the Major Research Instrumentation Program (NSF grant no. DMR-0958796). STEM analysis was carried out in the Characterization Facility of the University of Minnesota, which receives partial support from the NSF through the MRSEC program. The Acknowledgements were updated on December 17, 2014.

Received: July 27, 2014
Revised: August 24, 2014
Published online: September 30, 2014

[1] Q. H. Wang, K. Kalantar-Zadeh, A. Kis, J. N. Coleman, M. S. Strano, *Nat. Nanotechnol.* **2012**, *7*, 699.
[2] H. Guo, N. Lu, L. Wang, X. Wu, X. C. Zeng, *J. Phys. Chem. C* **2014**, *118*, 7242.
[3] R. Ionescu, W. Wang, Y. Chai, Z. Mutlu, I. Ruiz, Z. Favors, D. Wickramaratne, M. Neupane, L. Zavala, M. Ozkan, C. S. Ozkan, *TNANO* **2014**, *13*, 749.
[4] W. Ge, K. Kawahara, M. Tsuji, H. Ago, *Nanoscale* **2013**, *5*, 5773.

© 2014 WILEY-VCH Verlag GmbH & Co. KGaA, Weinheim

[5] Y.-H. Lee, X.-Q. Zhang, W. Zhang, M.-T. Chang, C.-T. Lin, K.-D. Chang, Y.-C. Yu, T.-W. Wang, C.-S. Chang, L.-J. Li, T.-W. Lin, *Adv. Mater.* **2012**, *24*, 2320.
[6] Y.-H. Lee, X.-Q. Zhang, W. Zhang, M.-T. Chang, C.-T. Lin, K.-D. Chang, Y.-C. Yu, J. T.-W. Wang, C.-S. Chang, L.-J. Li, T.-W. Lin, *Adv. Mater* **2012**, *24*, 2320.
[7] S. Kim, A. Konar, W. S. Hwang, J. H. Lee, J. Lee, J. Yang, C. Jung, H. Kim, J.-B. Yoo, J.-Y. Choi, Y. W. Jin, S. Y. Lee, D. Jena, W. Choi, K. Kim, *Nat. Commun.* **2012**, *3*, 1011.
[8] B. Radisavljevic, A. Radenovic, J. Brivio, V. Giacometti, A. Kis, *Nat. Nanotechnol.* **2011**, *6*, 147.
[9] Y. Yoon, K. Ganapathi, S. Salahuddin, *Nano Lett.* **2011**, *11*, 3768.
[10] J. Brivio, D. T. L. Alexander, A. Kis, *Nano Lett.* **2011**, *11*, 5148.
[11] J. Coleman, M. Lotya, A. O'Neill, S. Bergin, P. King, U. Khan, K. Young, A. Gaucher, S. De, R. Smith, I. Shvets, S. Arora, G. Stanton, H. Kim, K. Lee, G. Kim, G. Duesberg, T. Hallam, J. Boland, J. Wang, J. Donegan, J. Grunlan, G. Moriarty, A. Shmeliov, R. Nicholls, J. Perkins, E. Grieveson, K. Theuwissen, D. McComb, P. Nellist, *Science* **2011**, *331*, 568.
[12] Z. Zeng, Z. Yin, X. Huang, H. Li, Q. He, G. Lu, F. Boey, H. Zhang, *Angew. Chem. Int. Ed.* **2011**, *50*, 11093.
[13] S. Najmaei, Z. Liu, W. Zhou, X. Zou, G. Shi, S. Lei, B. I. Yakobson, J.-C. Idrobo, P. M. Ajayan, J. Lou, *Nat. Mater.* **2013**, *12*, 754.
[14] A. M. van der Zande, P. Y. Huang, D. A. Chenet, T. C. Berkelbach, Y. You, G.-H. Lee, T. F. Heinz, D. R. Reichman, D. A. Muller, J. C. Hone, *Nat. Mater.* **2013**, *12*, 554.
[15] J. Pütz, M. A. Aegerter, *J. Sol-Gel Sci. Technol.* **2000**, *19*, 821.
[16] J. Pütz, M. A. Aegerter, *J. Sol-Gel Sci. Technol.* **2003**, *26*, 807.
[17] K. Liu, W. Zhang, Y. Lee, Y. Lin, M. Chang, C. Su, C. Chang, H. Li, Y. Shi, H. Zhang, C. Lai, L. Li, *Nano Lett.* **2012**, *12*, 1538.
[18] Y.-C. Lin, W. Zhang, J.-K. Huang, K.-K. Liu, Y.-H. Lee, C.-T. Liang, C.-W. Chu, L.-J. Li, *Nanoscale* **2012**, *4*, 6637.
[19] S. Balendhran, J. Z. Ou, M. Bhaskaran, S. Sriram, S. Ippolito, Z. Vasic, E. Kats, S. Bhargava, S. Zhuiykov, K. Kalantar-Zadeh, *Nanoscale* **2012**, *4*, 461.
[20] H. Wang, L. Yu, Y.-H. Lee, Y. Shi, A. Hsu, M. L. Chin, L.-J. Li, M. Dubey, J. Kong, T. Palacios, *Nano Lett.* **2012**, *12*, 4674.
[21] R. J. Wu, M. L. Odlyzko, K. A. Mkhoyan, *Ultramicroscopy* **2014**, *147*, 8.
[22] K. P. Loh, L. K. Tan, B. Liu, J. Teng, S. Guo, H. Y. Low, *Nanoscale* **2014**, *6*, 10584.
[23] B. Li, S. Yang, N. Huo, Y. Li, J. Yang, R. Li, C. Fan, F. Lu, *RSC Adv.* **2014**, *4*, 26407.
[24] Z. Mutlu, D. Wickramaratne, H. H. Bay, Z. J. Favors, M. Ozkan, R. Lake, C. S. Ozkan, *Phys. Status Solidi A* **2014**, DOI: 10.1002/pssa.201431131.
[25] Z. Mutlu, M. Penchev, I. Ruiz, H. H. Bay, S. Guo, M. Ozkan, C. S. Ozkan, *MRS Proc.* **2012**, *1451*, 57.
[26] H. Li, Q. Zhang, C. C. R. Yap, B. K. Tay, T. H. T. Edwin, A. Olivier, D. Baillargeat, *Adv. Mater.* **2012**, *22*, 1385.
[27] R. Ionescu, A. George, I. Ruiz, Z. Favors, Z. Mutlu, C. Liu, K. Ahmed, R. Wu, J. S. Jeong, L. Zavala, K. A. Mkhoyan, M. Ozkan, C. S. Ozkan, *Chem. Commun.* **2014**, *50*, 11226.
[28] D. Wickramaratne, F. Zahid, R. K. Lake, *J. Chem. Phys.* **2014**, *140*, 124710.
[29] S. Mouri, Y. Miyauchi, K. Matsuda, *Nano Lett.* **2013**, *13*, 5944.
[30] U. Bhanu, R. I. Muhammad, L. Tetard, S. Khondaker, *Sci. Rep.* **2014**, *4*, 5575.
[31] R. Coehoorn, C. Haas, J. Dijkstra, C. J. F. Flipse, R. A. de Groot, A. Wold, *Phys. Rev. B* **1987**, *35*, 6195.
[32] Y. Zhan, Zheng Liu, S. Najmaei, P. M. Ajayan, J. Lou, *Small* **2012**, *8*, 966.
[33] J.-G. Song, J. Park, W. Lee, T. Choi, H. Jung, C. W. Lee, S.-H. Hwang, J. M. Myoung, J.-H. Jung, S.-H. Kim, C. Lansalot-Matras, H. Kim, *ACS Nano* **2013**, *7*, 11333.
[34] W. Zhao, Z. Ghorannevis, L. Chu, M. Toh, C. Kloc, P.-H. Tan, G. Eda, *ACS Nano* **2012**, *7*, 791.
[35] A. Berkdemir, H. R. Gutierrez, A. R.-Mendez, N. Perea-Lopez, A. L. Elias, C.-I. Chia, B. Wang, V. H. Crespi, F. Lopez-Urias, J.-C. Charlier, H. Terrones, M. Terrones, *Sci. Rep.* **2013**, *3*, 1755.
[36] H. R. Gutiérrez, N. Perea-Lopez, A. L. Elias, A. Berkdemir, B. Wang, R. Lv, F. Lopez-Urias, V. H. Crespi, H. Terrones, M. Terrones, *ACS Nano* **2013**, *7*, 11333.
[37] Y. Chen, J. Xi, D. O. Dumcenco, Z. Liu, K. Suenaga, D. Wang, Z. Shuai, Y.-S. Huang, L. Xie, *ACS Nano* **2013**, *7*, 4610.
[38] A. A. Jeffery, C. Nethravathi, M. l. Rajamathi, *J. Phys. Chem. C* **2014**, *118*, 1386.
[39] K. Kośmider, J. Fernández-Rossier, *Phys. Rev. Lett. B* **2013**, *87*, 075451.
[40] Y. Chen, J. Xi, D. O. Dumcenco, Z. Liu, K. Suenaga, D. Wang, Z. Shuai, Y.-S. Huang, L. Xie, *ACS Nano* **2013**, *7*, 4610.
[41] J. Mann, Q. Ma, P. M. Odenthal, M. Isarraraz, D. Le, E. Preciado, D. Barroso, K. Yamaguchi, G. von Son Palacio, A. Nguyen, T. Tran, M. Wurch, A. Nguyen, V. Klee, S. Bobek, D. Sun, T. F. Heinz, T. S. Rahman, R. Kawakami, L. Bartels, *Adv. Mater.* **2014**, *26*, 1399.

© 2014 WILEY-VCH Verlag GmbH & Co. KGaA, Weinheim